Sol-gel synthesis and characterization of undoped and Al-doped ZnO thin films for memristive application

Dawit G. Ayana, Valentina Prusakova, Cristian Collini, Marco V. Nardi, Roberta Tatti, Mauro Bortolotti, Leandro Lorenzelli, Andrea Chiappini, Alessandro Chiasera, Maurizio Ferrari, Lorenzo Lunelli, and Sandra Dirè

Citation: AIP Advances **6**, 111306 (2016); doi: 10.1063/1.4968192
View online: http://dx.doi.org/10.1063/1.4968192
View Table of Contents: http://scitation.aip.org/content/aip/journal/adva/6/11?ver=pdfcov
Published by the AIP Publishing

Sol-gel synthesis and characterization of undoped and Al-doped ZnO thin films for memristive application

Dawit G. Ayana,[1,a] Valentina Prusakova,[1] Cristian Collini,[2] Marco V. Nardi,[1,3] Roberta Tatti,[3] Mauro Bortolotti,[1] Leandro Lorenzelli,[2] Andrea Chiappini,[4] Alessandro Chiasera,[4] Maurizio Ferrari,[4] Lorenzo Lunelli,[5] and Sandra Dirè[1]
[1]*Department of Industrial Engineering, University of Trento, Via Sommarive 9, 38123 Trento, Italy*
[2]*FBK, CMM - MICROSYSTEMS, Via Sommarive 18, 38123 Trento, Italy*
[3]*CNR-IMEM, Via Alla Cascata 56/C, 38123 Trento, Italy*
[4]*CNR-IFN, CSMFO Lab., Via Alla Cascata 56/C, 38123 Trento, Italy*
[5]*FBK, LaBSSAH, Via Sommarive 18, 38123 Trento, Italy*

(Received 29 July 2016; accepted 5 November 2016; published online 15 November 2016)

The Sol-gel route is a versatile method to fabricate multi-layer, dense and homogeneous ZnO thin films with a controlled thickness and defects for a memristive application. In this work, sol-gel derived multi-layer undoped and Al-doped ZnO thin films were prepared by a spin-coating technique on SiO_2/Ti/Pt and silica glass substrates. The effect of both Al doping and curing conditions on the structural and morphological features of ZnO films was investigated by complementary techniques, including electron microscopy, atomic force microscopy, X-ray photoelectron spectroscopy, micro-Raman spectroscopy, and X-ray diffraction analysis. Electrical measurements were performed on SiO_2/Ti/Pt/ZnO/Pt(dishes) and SiO_2/Ti/Pt/ZnO(Al)/Pt(dishes) fabricated memristive cells and preliminary current-voltage curves were acquired. [http://dx.doi.org/10.1063/1.4968192]

INTRODUCTION

A memristor is a fourth fundamental circuit element that was predicted by L. Chua in 1971.[1] The first TiO_2-based memristor was fabricated by HP lab in 2008 as a physical model of a two terminal electrical device.[2] Ever since then, a wide range of materials, have been studied for potential application as a resistive switching layer,[3,4] and numerous authors reported on memristive behavior in ZnO-based devices.[5–9] The sol-gel fabrication is a cost-efficient method that provides a possibility to deposit thin films even on a large area.[10] Although there are only few reports regarding sol-gel derived ZnO thin films with a memristive response,[11,12] the wet chemical method is a promising technique that provides a control over variety of properties, including stoichiometry, porosity, crystallinity, and morphology.[13] In order to obtain reproducible current-voltage switching cycles with the absence of short circuits, the obtained layers should be dense, free of holes and cracks and have a constant thickness through the films. Accordingly, we have recently exploited the sol-gel route for the production of dense and defect-free ZnO layers for memristive applications[14,15] by optimizing both synthesis and processing conditions.

Several modification approaches were proposed to improve the resistive switching performance of ZnO thin films.[16–19] For instance, doping was used to improve the electrical and optical properties of sol-gel derived ZnO films for different applications.[13,20–22] Replacing Zn^{2+} ions by cations of higher oxidation states, such as Al^{3+}, in a ZnO lattice alters an electrical conductivity by increasing electronic charge carriers density. Moreover, an addition of Al^{3+} ions to Zn^{2+} sol solution increases the number of nucleation sites, resulting in higher grain boundary density

[a]Corresponding author: dawitgemechu.ayana@unitn.it

and the formation of smaller grains.[13] Grain boundaries are anticipated to improve a memristive switching process, providing sites with defect aggregation and a conductive path formation in HfO_2, as was previously published.[23] Additionally, Al-doped ZnO thin film-based device showed a better yield, which was attributed to an excellent interface quality between electrodes and films.[24]

In this study, undoped, 0.5 and 1 at.% Al-doped ZnO thin films were fabricated by the sol-gel technique. The effects of doping and curing conditions on the morphological and structural properties, influencing the memristive switching performance of ZnO layers, were analyzed. Preliminary electrical measurements were performed on undoped and 0.5 % Al-doped ZnO layers sandwiched between platinum electrodes.

EXPERIMENTAL PART

The synthesis of undoped ZnO sol was previously reported.[14,15] The Al-doped ZnO sols were obtained by a drop-wise addition of monoethanolamine (MEA) to a 0.1 M solution of zinc acetate dihydrate (ZAD), in ethanol (ZAD:MEA = 1:0.5 molar ratio) followed by aluminum isopropoxide addition (0.5 and 1 at. % Al-doped sols). The resulting mixtures were refluxed under stirring at 80 °C for 2 h and cooled down to room temperature (RT). Multilayered films (8 layers) were obtained by spin coating from undoped and Al-doped ZnO sols on silica and oxygen plasma treated $Pt/Ti/SiO_2$ substrates.[14,15] After each layer deposition, the films were cured in an atmosphere of air either at 250 °C for 1 h (samples A) or 300 °C for 10 min (samples B). Finally, the films were annealed at 400 °C for 4 h with a heating/cooling rate of 1 °C/min.

Field emission scanning electron microscopy (FE-SEM) was performed on a Joel JSM-7401F. Atomic force microscopy (AFM) data were acquired using an Asylum Research Cypher equipped with the Environmental Scanner module. Optical transmission measurements were performed on the films deposited on silica substrates using a double beam Cary Varian-5000 spectrophotometer. The optical parameters of the films were estimated using Point-wise Unconstrained Optimization Approach (PUMA).[25] X-ray photoelectron (XPS) and ultraviolet photoelectron spectroscopy (UPS) were performed with CLAM2 Electron Hemispherical Analyzer. Monochromatic MgKα excitation with energy of 1253.6 eV was used as an X-ray source for XPS analysis, and a helium discharge lamp at 21.22 eV was used for UPS analysis. X-ray diffraction (XRD) analyses were acquired on an Italstructures IPD3000 instrument equipped with a Cu anode source. The measurements were performed in a glancing incidence mode (3°) with respect to the incident beam, and spectra were collected with an Inel CPS120 detector. Micro-Raman spectra were recorded by a Labram Aramis instrument using 632.8 nm He-Ne laser as excitation source and a holographic grating with 1800 grooves/mm. Electrical measurements were performed with Pt dishes (260±10 μm in diameter, 40±2 nm thick) as top electrodes deposited by the electron beam evaporation.[26] The current-voltage (I-V) characteristics were acquired at RT in a presence of LED light with a custom setup, composed of NI PXIe-1073 chassis (equipped with NI-PXIe-4139 source measure) connected to a PC through a PCI-express card and controlled by a software user interface developed within the Labview environment.

RESULTS AND DISCUSSION

The morphological features of the films deposited on $Pt/Ti/SiO_2$ substrates were analyzed by FE-SEM, yielding detailed information regarding the influence of doping and curing conditions on the morphology of the films (Fig.S1 - supplementary material). Undoped ZnO films' surfaces (Fig.S1a, sample A) revealed a presence of spherical grains, which were estimated to have an average size of about 40 nm, with residual inter-grain porosity. Doping ZnO films with 0.5% Al (Fig.S1b) led to decrease both inter-grain porosity and grain size (about 10 nm). An increase of the grain size up to approximately 25 nm was observed with 1% Al sample (Fig.S1c) cured at 250°C. The different curing conditions seem not to affect the morphology of the undoped ZnO films (Fig.S1d). For samples cured at 300 °C (Fig.S1 (e-f)), doping with Al leads again to the decrease in grain size respect to undoped ZnO but no significant differences can be observed in

FE SEM micrographs between 0.5 and 1% Al-doped samples. The FE-SEM images of samples B (Fig.S1 (d-f)) point out that Al-doped samples cured at 300 °C display larger grains than those cured at 250°C.

Fig. 1(a–c) shows the AFM images of samples A, revealing the reduction of the grain size upon 0.5 % Al doping compared to undoped or 1 % doped films (Table SI- supplementary material), in agreement with FE-SEM data.

The surface roughness increased upon doping with 1% Al compared to the 0.5 % doped samples. The AFM images of samples B (Fig. 1 (d–f)) confirmed the trend of samples A, indicating that doping with 0.5% Al (Fig. 1e) leads to smaller grains and lower surface roughness (Table SI). Contrary to the FE SEM results, the grain diameter appears larger in 1% Al-doped than in 0.5% Al-doped sample, with more evident uneven size distribution.

Both FE-SEM and AFM data suggest that the grain size of samples B was relatively larger than that of samples A. In general, smaller grains size and even grain distribution with uniform surface morphology and reduced surface roughness were observed in Al-doped films.

PUMA software was used to estimate thickness and refractive index of the films from the transmission spectra (Table SII). The porosity of the samples was determined using the approach discussed in Ref. 27, assuming the reference refractive index of ZnO film at 632.8 nm as 1.989. Al-doped ZnO films displayed lower porosity (Table SII) respect to the undoped samples, confirming that an addition of Al modifies the morphology and grain size, in general agreement with the morphological analysis above. The 0.5% Al-doped sample B displayed a porosity of 5% and thickness of 83 nm.

The XPS survey spectra acquired from all the films (Fig. S2) showed no other contamination apart that from atmosphere (C 1s signal). Fig. 2 shows the XPS Zn2p and Al2p spectra. The Zn 2p spectra in Fig.2 contain two peaks identified as Zn 2p3/2 and Zn 2p1/2. The O1s core level spectrum (Fig. S3- supplementary material) exhibits the expected line shape with a main peak centered at BE of 531 eV, which can be attributed to the bulk oxygen, and a shoulder at higher BE (i.e. 532.5 eV) related to the oxygen from the surface of the film.

The Zn 2p signal shows no change with respect to the level of Al doping, which points toward an Al doping that was most probably interstitial. The Al 2p core levels are detectable in all Al-doped ZnO films. The signal corresponding to Al shows an increase in the intensity according to the nominal amount of Al doping. The work functions were calculated from the UPS spectra (not shown). For samples B, the work functions were 4.20, 4.35 and 4.50 eV, for 0, 0.5% and 1% Al,

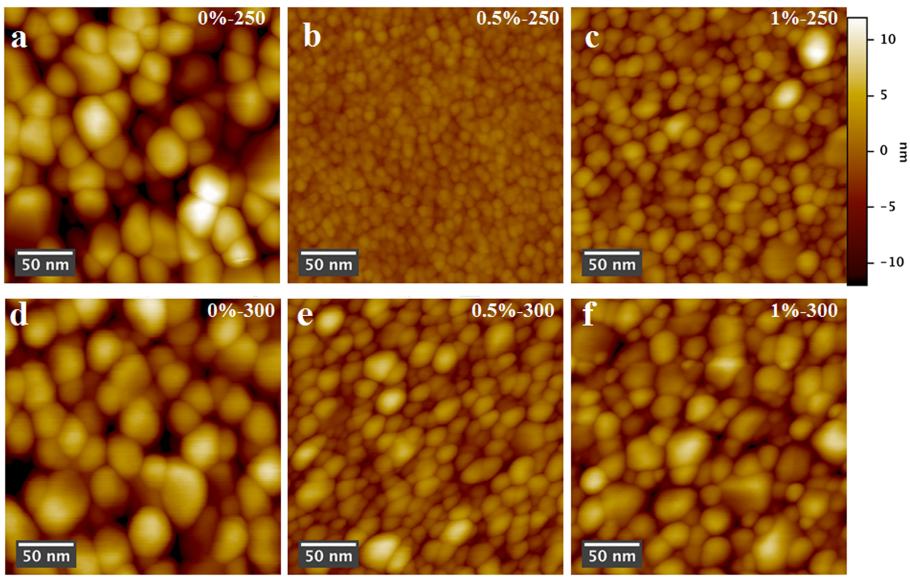

FIG. 1. AFM images of undoped, 0.5 % and 1% Al-doped ZnO films: samples A (a-c) and B (d-f).

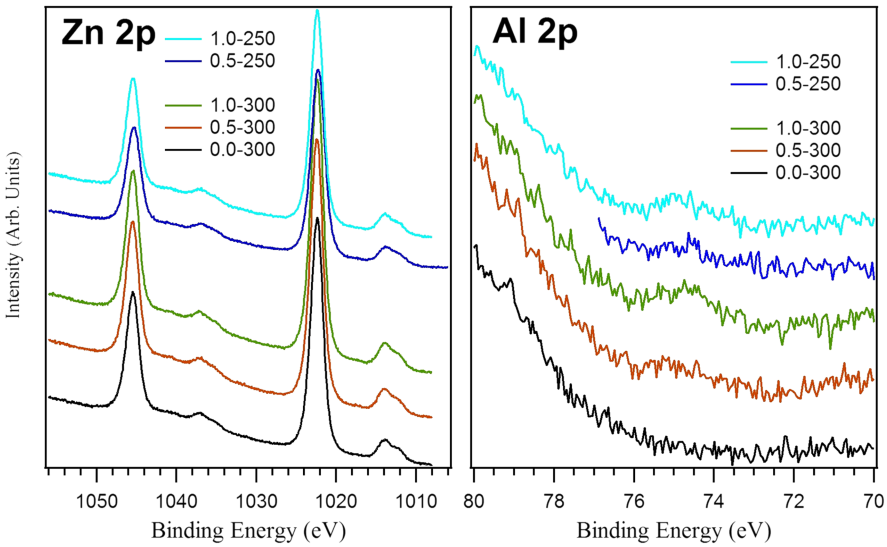

FIG. 2. XPS Zn2p and Al2p core level spectra of samples B and doped samples A.

respectively. Likewise, the work functions of the 0.5 and 1% Al-doped (samples A) were 4.2 and 4.25 eV, correspondingly. The increase in the work functions is coherent with the Al levels, indicating the effectiveness of Al-doping, in particular, for the samples B.

XRD spectra were acquired from the films deposited on $Pt/Ti/SiO_2$ substrates and cured at 300 °C (Fig.S4 - supplementary material), and data were analyzed using the Maud software,[28] adopting a full-pattern quantitative modeling approach based on the Rietveld method. The XRD patterns of samples A were similar regardless of the curing conditions. The substrate contributed to the XRD spectra with the broad halo at 20-30º due to amorphous SiO_2 and Pt strong reflections. All the films were crystalline with the ZnO hexagonal wurtzite structure. The absence of peaks characteristic of Al related phases in doped samples indicates interstitial substitution of Zn^{2+} by Al^{3+} as a predominant effect for both 0.5% and 1% Al doping levels. The average crystalline domains' dimension was determined by a Lorentzian broadening model, assuming an isotropic shape, as described in Ref. 29 and implemented in the Maud software (Table SI). Doping with Al leads to a decrease in the crystallite size, ascribable to the difference between the ionic radius of Zn and Al.[19]

Fig.3 (a) shows the Raman spectra of undoped ZnO films cured at 250 °C and 300 °C.

The main peaks are characteristic of the wurtzite phase. Relative intensities and peak positions of both samples are comparable indicating that the intermediate curing parameters display the absence of prominent effect on the final structure of the films. Raman spectra were also recorded on Al-doped ZnO films cured at 250 °C (not shown) and 300 °C. Fig.3 (b) presents the Raman spectra of samples B. A relative peak shift and broadening of the E_2 $^{(high)}$ band, with respect to the usual position of ZnO thin film at 437cm^{-1},[30] were observed in 0.5% and 1% Al-doped ZnO samples, and attributed to a decreased degree of order in the wurtzite phase. Moreover, an increase in the intensity of the longitudinal optical (LO) band at 578 cm^{-1} and the decrease of the E_2 $^{(high)}$ band were detected and can be attributed to both the formation of defects, such as oxygen vacancies,[31,32] and the modification of the ZnO crystalline lattice due to a dopant inclusion.[33]

The current-voltage (I-V) characteristics of $Pt/ZnO/Pt/Ti/SiO_2$ and $Pt/ZnO(Al)/Pt/Ti/SiO_2$ memristive cells are presented in Fig. 4. No electroforming was required for both 0.5 % Al-doped and undoped ZnO thin films sandwiched between platinum electrodes. Current compliances of up to 15 mA and 30 mA were tested for undoped and 0.5 % Al-doped ZnO-based device, correspondingly, with the absence of a breakdown in the memristive cells and damage of top electrodes during the measurements. Both undoped and 0.5 % Al-doped ZnO-based devices displayed a pinched hysteresis loop centered at the origin, which is a fingerprint of a memristive switching behavior.[34]

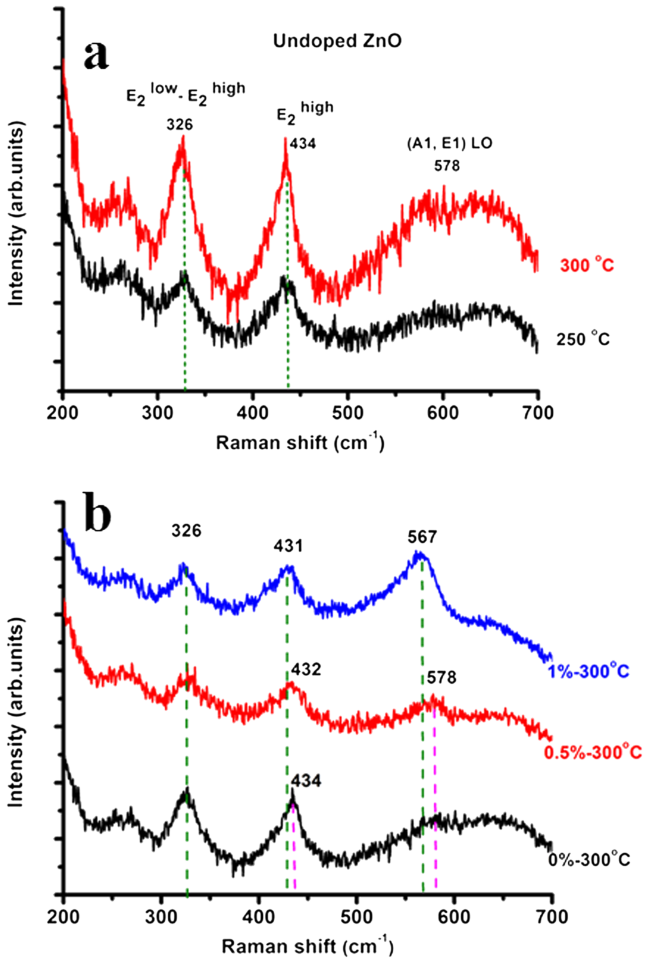

FIG. 3. a) Raman spectra of undoped ZnO films cured at 250 °C and 300 °C b) Raman spectra of samples B.

Resistance values at high resistance state (HRS) and low-resistance state (LRS) were reduced in 0.5 % Al-doped ZnO-based devices compared to those obtained from the undoped materials. An electrical response of a cell is strongly dependent on a structure of a switching layer and its interface with an electrode. The sol-gel method provides a fine convenient control over film morphology by adjusting synthetic or processing conditions. Therefore, by simply tuning the sol-gel parameters it is possible to obtain films with the desired switching characteristics.

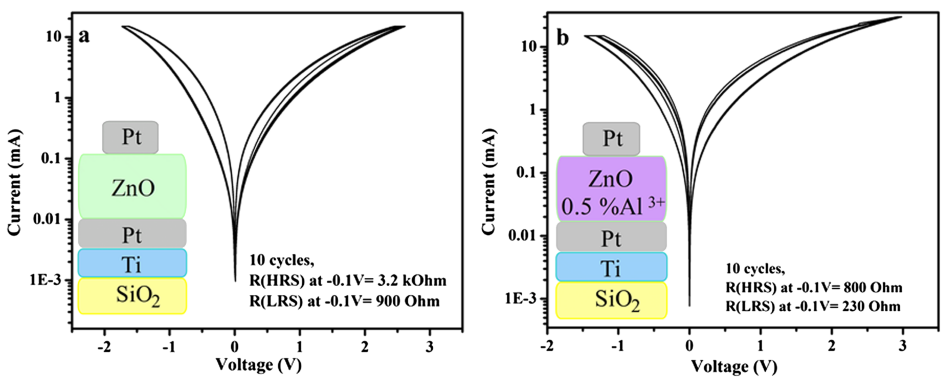

FIG. 4. I-V curves of a) undoped and b) 0.5% Al-doped ZnO thin films cured at 300 °C.

CONCLUSION

Sol-gel derived ZnO thin films were prepared by the spin coating technique. Both curing conditions and Al-doping were found to modify film's morphology and grain sizes. Doping ZnO films with Al resulted in a reduction of surface roughness and grain size, that is most prominent at 0.5 at. %. Although the ZnO wurtzite crystalline phase was the only one detected in all films, micro-Raman data revealed a decreased order of the hexagonal phase in Al-doped samples. Al was doped interstitially and increased the work functions, in particular, for samples cured at 300°C. The reduction of porosity, surface roughness and grain size of films obtained by Al-doping appear promising for the fabrication of dense switching layers.

SUPPLEMENTARY MATERIAL

See supplementary material for FE-SEM images (FIG.S1), Table SI (roughness, equivalent diameter and crystallite size of the ZnO films), Table SII (thickness, refractive index and porosity of the films), XPS survey spectra (FIG. S2), XPS O1s core level spectrum (FIG. S3) and XRD spectra of ZnO films (FIG. S4).

ACKNOWLEDGMENTS

This work has been supported by Province of Trento (Call 2012-Grandi Progetti PAT) in the framework of the project MaDEleNA. Prof. Luca Lutterotti (University of Trento, Department of Industrial Engineering) is acknowledged for the acquisition of X-ray diffraction. The authors also would like to thank Dr. Mario Barozzi for the acquisition of FE-SEM images (CMM-MNF).

[1] L. O. Chua, IEEE Trans. Circuit Theory **18**, 507 (1971).
[2] D. B. Strukov, G. S. Snider, D. R. Stewart, and R. S. Williams, Nature **453**, 80 (2008).
[3] P. Wong, H. Y. Lee, S. Yu, Y. S. Chen, Y. Wu, P. S. Chen, B. Lee, F. T. Chen, and M. J. Tsai, Proceedings of the IEEE **100**, 1951 (2012).
[4] A. Janotti and C. G. Van deWalle, Rep. Prog. Phys. **72**, 126501 (2009).
[5] S.-C. Qin, R.-X. Dong, and X.-L. Yan, Appl. Phys. A **116**, 1 (2014).
[6] N. M. Muhammad, N. Duraisamy, K. Rahman, H. W. Dang, J. Jo, and K. H. Choi, Current Applied Physics **13**, 90 (2013).
[7] N. Xu, L. Liu, X. Sun, X. Liu, D. Han, Y. Wang, R. Han, J. Kang, and B. Yu, Appl. Phys. Lett. **92**, 232112 (2008).
[8] N. Xu, L. F. Liu, X. Sun, C. Chen, Y. Wang, D. D. Han, X. Y. Liu, R. Q. Han, J. F. Kang, and B. Yu, Semicond. Sci. Technol. **23**, 075019 (2008).
[9] W. Y. Chang, Y. C. Lai, T. B. Wu, S. F. Wang, F. Chen, and M. J. Tsai, Appl. Phys. Lett. **92**, 022110 (2008).
[10] L. Znaidi, Mater. Sci. Eng., B **174**, 18 (2010).
[11] N. A. A. Shaari, S.M.M. Kasim, N. S. M. Sauki and S. H. Herman, Mater. Sci. Eng. **99**, 012022 (2015).
[12] S. Kim, H. Moon, D. Gupta, S. Yoo, and Y. K. Choi, IEEE Transactions on Electron Devices **56**, 696 (2009).
[13] S. Salam, M. Islam, and A. Akram, Thin Solid Films **529**, 242 (2013).
[14] D. G. Ayana, V. Prusakova, R. Ceccato, C. Collini, L. Lorenzelli, and S. Dirè, Thin solid Films **615**, 427 (2016).
[15] D. G. Ayana, V. Prusakova, R. Ceccato, and S. Dirè, AISEM Annual Conference 2015 XVIII (2015).
[16] J. L. Shi, D. S. Shang, Y. S. Chen, J. Wang, J. R. Sun, and B. G. Shen, Phys. D: Appl. Phys. **44**, 455305 (2011).
[17] J. Qiu, A. Shih, W. Zhou, Z. Mi, and I. Shih, J. Appl. Phys. **110**, 014513 (2011).
[18] Y. Sun, X. Yan, X. Zheng, Y. Liu, Y. Zhao, Y. Shen, Q. Liao, and Y. Zhang, ACS Appl. Mater. Interfaces **7**, 7382 (2015).
[19] K. Kinoshtia, T. Okutani, H. Tanaka, T. Hinoki, K. Yazawa, K. Ohmi, and S. Kishida, Appl. Phys. Lett. **96**, 143505 (2010).
[20] P. Nunesa, E. Fortunatoa, P. Tonelloa, F. B. Fernandesa, P. Vilarinhob, and R. Martinsa, Vacuum **64**, 281 (2002).
[21] M. Rezaee, M. Behdani, H. Arabshahi, and N. Hosseini, International Review of Physics **12**, 105 (2009).
[22] M. Rydzek, M. Reidinger, M. Arduini-Schuster, and J. Manara, Progress in Organic Coatings **70**, 369 (2011).
[23] K. McKenna and A. Shluger, Appl. Phys. Lett. **95**, 222111 (2009).
[24] D. Lee, D. K. Hwang, M. Chang, Y. Son, D. Seong, D. Choi, and H. Hwang, *IEEE 2006 International Electron Devices Meeting* (2006), p. 1.
[25] E. G. Birgin, I. Chambouleyron and J. M. Mart′ınez, Journal of Computational Physics **151**, 862 (1999).
[26] V. Prusakova, C. Collini, L. Pasquardini, L. Vanzetti, G. Resta, C. Pederzolli, L. Lorenzelli, and S. Dirè, AISEM Annual Conference 2015 XVIII (2015).
[27] V. Prusakova, C. Armellini, A. Carpentiero, A. Chiappini, C. Collini, S. Dirè, M. Ferrari, L. Lorenzelli, M. Nardello, S. Normani, A. Vaccari, and A. Chiasera, Phys. Status Solidi C **12**, 192 (2015).
[28] L. Lutterotti, M. Bortolotti, G. Ischia, I. Lonardelli, H. R. Wenk, and Z. Kristallogr, Suppl. **26**, 125 (2007).
[29] R. Delhez, Th.H. de Keijser, J. I. Langford, D. Louër, E. J. Mittemeijer, and E. J. Sonneveld, *International Union of Crystallography*. Oxford Science Publications **132** (1993).
[30] V. Russo, M. Ghidelli, P. Gondoni, C. S. Casari, and A. Li Bassi, J. Appl. Phys. **115**, 073508 (2014).

[31] S. B. Yahiaa, L. Znaidia, A. Kanaeva, and J. P. Petitet, Spectrochimica Acta Part A **71**, 1234 (2008).
[32] S. H. Jeong, J. k. Kim, and B. T. Lee, J. Phys. D: Appl. Phys. **36**, 2017 (2003).
[33] M. F. Cerqueira, T. Viseu, J. Ayres de Campos, A. G. Rolo, T. de Lacerda-Aroso, F. Oliveira, I. Bogdanovic-Radovic, E. Alves, and M. I. Vasilevskiy, Phys. Status Solidi A **212**, 2345 (2015).
[34] L. Chua, Semicond. Sci. Technol. **29**, 104001 (2014).